Steam - Oxygen Gasification of refuse derived fuel in fluidized beds: modelling and pilot plant testing

Alex Sebastiani[a], Domenico Macrì[a], Katia Gallucci[b], Massimiliano Materazzi[a,*]

[a] Department of Chemical Engineering, University College London, London WC1E 7JE, UK

[b] Department of Industrial Engineering and Information and Economy, Monteluco di Roio, 67100 L'Aquila, Italy

[*] Corresponding author.

E-mail address: massimiliano.materazzi.09@ucl.ac.uk

ABSTRACT

A one-dimensional kinetic model for steam-oxygen gasification of refuse derived fuel in a bubbling fluidized bed reactor has been developed. The model incorporates the reaction network of steam-oxygen gasification within the fluid dynamics of a fluidized bed to predict waste and tars conversion, gas composition and overall gasification performance. The model was validated by comparing outlet products composition and temperature profile with experimental data from a pilot-scale fluidized bed gasifier, operated at different conditions. The model showed accurate predictive capability and ease of computation. The effects of the operating conditions on gas yield and process efficiency were evaluated and the most appropriate fuel feeding height, equivalent ratio and the relative amount of steam to inject were identified.

KEYWORDS

Waste gasification, fluidized-bed, thermochemical treatment, kinetic model

1 INTRODUCTION

Finding solutions to the problems associated to municipal solid waste (MSW) disposal, along with the requirement of reliable and abundant sources of renewable energy are the pillars of the current environmental agendas of many developing and developed countries. The combination of renewable energy requirements, decarbonisation and diversion of materials from landfills have recently led to focus on the use of residual biomass and waste as source of renewable energy or chemical feedstock [1,2]. This would serve the purpose of meeting the increased energy demand (via energy or alternative fuels production), as well as that of avoiding dispersion of problematic contaminants in the environment by favouring the chemical recycling. One possible way to achieve this is by intensifying the use of advanced thermochemical technologies (ATT) and, amongst all the available options, gasification represents the most promising in terms of waste reduction and energy efficiency, as well as versatility of operating conditions and large number of possible applications [3–5]. The feedstock for ATT consists of residues from mechanical treatment of MSW, upon removal of recyclable materials, shredding and, when required, enhanced drying. The residual material is known as refuse derived fuel (RDF), which has a significant energy content (approximately 20 MJ/kg) and great potential for energy recovery and landfill diversion [6,7]. The greatest technical challenge to overcome for the successful growth of commercial RDF gasification technologies is that of achieving a quality of syngas that is good enough to sustain a stable and long-term operation of high-efficiency energy devices (e.g. fuel cells) or catalytic reactors for

synthetic fuels [8–10]. The latter, in particular, requires a gas of adequate H_2:CO ratio, and the absolute absence of tar species and other catalyst polluters, such as sulphur and chlorine, that would damage the catalysts [11,12]. In many cases, nitrogen dilution in the syngas should also be avoided to reduce the cost of compression and simplify the gas separation downstream. This is particularly true in new ATT applications for biohydrogen and bioSNG production [13–15], which are gaining great attention in Europe [16]. Additional challenges are related to process scalability and flexibility, both necessary conditions for operation on waste feedstock. Within this context, fluidised bed reactors have proved to be particularly suitable for ATT of low-quality feedstock, as proven by several pilot and demonstration-scale operations in the last decade [12,14,17–19]. In particular, steam and steam-oxygen gasification in fluidised beds are attracting interest for their good performance and high quality syngas that, differently from that of traditional air-blown gasifiers, has higher calorific value as virtually nitrogen-free [20].

Despite this growing attention to steam-oxygen gasification of biogenic residues and waste feedstock, literature and industrial reference to this technology are still very scarce, both from modelling and experimental perspectives [21–23]. In order to investigate and overcome all the challenges related to the process, a mathematical model for steam-oxygen gasification can be built assuming either thermodynamic equilibrium or reaction kinetics. Despite being simpler and faster from a computational point of view, equilibrium models can produce unreliable results, as they would only predict the maximum (theoretical) yields. On the other hand, a multidimensional model, which accounts for the reactor geometry and process fluid dynamic, along with selected reaction kinetics, gives more accurate results. This kind of models is based on equations of change and require a numerical approach to be solved. The higher reliability, however, implies higher complexity, as well as larger computational times that limit their application.

Different models have been proposed, both based on thermodynamic equilibrium [24–27] or kinetic considerations [28–30] but most of these are developed for a biomass feeding and their applicability to waste-derived fuel is not straightforward. Amongst the kinetic models, Oyedeji and Adboulmoumine [31] have developed a CFD-DEM model to investigate the effect of contaminants on the performance of biomass gasification. Despite being accurate in representing the fluid dynamic of the gasifier, the CFD-DEM model requires extensive computational resources and time to simulate the process.

Agu et al. [32] developed a one-dimensional unsteady state model for steam-biomass gasification in a bubbling fluidized bed (BFB) that includes also momentum balances of particles. The mono-dimensional approach proved to be computationally less demanding without losing accuracy and predictive capability of the effect of feeding position. A similar approach was used by Kaushal et al. [33] to model biomass gasification in a BFB gasifier, where the two phases theory was used to describe the BFB. Gomez-Barea and Leckner [34] adopted a different method to develop a model to predict the conversion of biomass in a FBG. They used a quasi-equilibrium approach using an equilibrium sub-model to calculate the gas composition. These are then corrected with kinetics sub-models that deviate the results from equilibrium. The modular structure provided flexibility to the model.

From the available literature, it is evident that a kinetics-based, mono-dimensional approach appears to offer the best compromise between accuracy and computational complexity, while a modular structure gives the flexibility needed for different applications. Real plants data, however, are necessary to validate these models, especially for novel applications using waste feedstock and steam-oxygen operation.

The overarching objective of this work is to develop and test a one-dimensional non-isothermal kinetic model for steam-oxygen gasification of RDF in a BFB, to quickly predict process efficiency and performance at different operating conditions. The model is validated

with real data from a steam-oxygen waste gasification plant in Swindon (UK). Operation of the plant was aimed at producing a syngas of consistent, reproducible and acceptable quality (i.e. suitable, after refining and further cleaning, for ultimate use as a feed to a catalytic reactor) with high gasification yields and minimum nitrogen content. Finally, the model is utilised to gain a better understanding of the operating capabilities of the BFB reactor and to establish whether there is an agreement between theoretically predicted and observed values (in terms of oxygen/steam flow rates, energy input, gas compositions/flow rates).

2 MODEL DESCRIPTION

The model described in this study for the gasification process is based on chemical reaction kinetics, coupled with the typical features of a BFB. The whole gasifier is divided into two different sections: the bottom zone, which represents the BFB, and the top of the reactor, which represents the freeboard section. The freeboard is modelled as a homogeneous plug flow reactor (PFR), the bed zone is described according to the two-phase theory [35]. An overview of the discretized fluidized bed gasifier (FBG) structure is shown in Figure 1. To simplify the computational load of a kinetic model and handling of the phenomena involved in the process, it is assumed that there are no variations of temperature and concentrations in the radial direction; therefore, the model is one-dimensional and predicts changes only in the axial direction. The height of the bed has been divided into a series of compartments of suitable finite volume where the set of differential equations of mass and energy balances are solved. The discretisation of the solutions could affect the accuracy of the model; therefore, the grid size has been chosen as an optimized compromise between precision and computational time. Mass and energy balances are solved in each compartment, whereas the output solution is used as input of the subsequent one. This discretisation also allows having the fuel feeding point as a variable input datum. The model is further simplified by decoupling primary decomposition

and secondary conversion of RDF feedstock. Primary decomposition includes devolatilization of the fuel particle in absence of oxygen, while the subsequent conversion consists mostly of extra particle reactions like oxidation, cracking and reforming of the gas species [36]. The two phenomena are considered to occur in series and have been investigated separately.

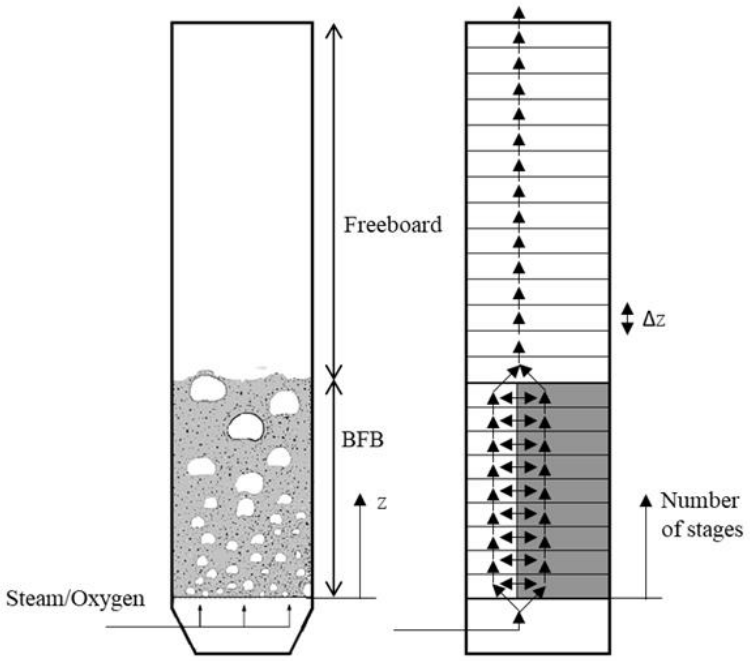

Figure 1 – Compartment structure of the model.

2.1 Primary RDF decomposition

When RDF enters the reactor it immediately undergoes drying (i.e. release of the moisture content), and devolatilization, by which RDF is broken into lighter molecules. The products of the primary decomposition are assumed to be gas/vapour species (i.e. volatiles), and char (section 2.3.2). The two processes start at low temperatures (100°C and 350°C respectively) and they are enhanced and accelerated by rising the temperature of the reactor [37]. The chemical reactions and processes should be predicted quantitatively, but due to the complexity of the conversion and the phenomena involved, suitable simplifications have to be developed [36]. The first assumption is that the quantity of moisture in the RDF is quickly released as vapour, adding to the inlet steam content. The products of devolatilization are also often

assumed to be released instantaneously, as reported by many authors [38–41]. Aghaalikhani et al. [27] proposed a detailed model of biomass gasification in ASPEN plus environment, showing the crucial role played by pyrolysis. In their approach, the pyrolytic products are char and volatiles, and yields of gas at different temperature have been used to quantify the amount of volatiles released. Others, like Kaushal et al. [33] model the biomass char as a partly volatile fuel, and the products of devolatilization are added to the up-flowing gas stream in a predefined pattern to avoid destabilizing effects to the hydrodynamic of the BFB.

The kinetic of devolatilization and the resulting product yields are fuel-specific and depend on process conditions, such as temperature and heating rates [34]. Cozzani et al. [42] studied the devolatilization behaviour of RDFs under heating conditions of conventional pyrolysis processes, determining the product yields and gas composition over a wide range of temperatures. In this work, a similar approach is followed to determine the overall primary decomposition reaction and products distribution (as char, moisture, gases and tars). The tar fraction is further divided into naphthalene (representative of multi-aromatic species) and a primary lumped tar component. Both are then subject to thermal cracking and reforming reactions to yield more gas or secondary tars [43]. The initial gas fraction is composed of hydrogen, carbon monoxide, carbon dioxide, methane and benzene according to Eq. 1. The yields of each devolatilization product are obtained from data in section 2.3.2. The solid residue is composed of carbon and ashes, the latter considered inert.

$$RDF \rightarrow \alpha H_2 + \beta H_2O + \gamma CO + \zeta CO_2 + \omega CH_4 + \vartheta C_6H_6 + \eta C_{10}H_8 + \xi tar + \kappa char \quad (1)$$

2.2 Computational model formulation

The two-phase model assumes that the fluidised bed consists of two phases: the emulsion phase and the bubble solid-free phase. All gas in excess of that required for minimum fluidising condition passes through the bed as bubbles [44]. The bed material (typically sand) is considered to be inert and there is no mass loss due to entrainment of sand particles. This

assumption allows to consider the bed height as a constant parameter. In reality, particle size distribution of bed material changes over time, and particles elutriation can occur to varying extent depending on fines fraction, which for simplicity was not considered in this model. The RDF residual solid fraction (i.e. carbon and ashes in char, after devolatilization) is added to the emulsion phase. In particular, while the ashes are considered to be inert, the carbon in char coarse particles is exposed to heterogeneous reactions ($r_{12\text{-}14}$ in Table 3). A fraction of char particles can elutriate with the gas flow depending on particle size [45,46].

The whole gasification process is strongly affected by the temperature that influences the reaction kinetics therein and regulates diffusion phenomena. In this model, it is assumed that both the heterogeneous and the homogeneous reactions take place only in the emulsion phase of the bed. The mass transfer is responsible for the exchange of gas species across the boundary between bubble and emulsion phase and, therefore, it occurs as long as a concentration gradient exists.

The rate of change in concentration of the i-th species, in both emulsion and bubble phases and the freeboard section, is expressed by Equations 2-4:

Emulsion phase (e) $$\frac{dc_{ei}}{dz} = \frac{\delta}{1-\delta}\frac{K_{be}\varepsilon_e}{u_e}(c_{bi} - c_{ei}) + \frac{\varepsilon_e}{u_e}\sum_j \nu_{i,j}\, r_j \quad (2)$$

Bubble phase (b) $$\frac{dc_{bi}}{dz} = \frac{K_{be}}{u_b}\,(c_{ib} - c_{ie}) \quad (3)$$

Freeboard (f) $$\frac{dc_{fi}}{dz} = \frac{1}{u_f}\sum_j \nu_{i,j}\, r_j \quad (4)$$

Where K_{be} is the interchange coefficient between bubble and emulsion phase [35]. The meaning of symbols can be found in the nomenclature section at the end.

One of the main advantages of a fluidised bed is a good solid mixing due to the upward gas stream that globally results in temperature homogeneity across the whole bed [47]. This is also promoted by the large contact surface and the high heat exchange rates between gas and solid

particles. For these reasons, the emulsion phase is modelled as isothermal. This assumption will be verified in the results section.

In the freeboard, the temperature profile is affected by chemical reactions and heat losses. Energy balances for emulsion and bubble phases and the freeboard are expressed by Equations 5-7

Emulsion phase (e)	$\frac{dT_e}{dz} = 0$	(5)
Bubble phase (b)	$\frac{dT_b}{dz} = \frac{H_{be}}{u_b} \cdot \frac{1}{\sum_i c_{bi} c_{pi}} (T_e - T_b)$	(6)
Freeboard (f)	$\frac{dT_f}{dz} = \frac{1}{\sum_i c_{fi} c_{pi}} \frac{1}{u_f} \left(\sum_j r_j \Delta H_j^r - \frac{(T_f - T_a)}{R_{tot}} \right)$	(7)

Where R_{tot} is the total thermal resistance to the heat losses due to the insulation. Expressions for the heat of reaction ΔH_j^r and heat capacities c_{pi} are taken from literature [48] and can be found in the *Supplementary material*.

The correlations in Table 1 describe the bubble rise velocity and other fundamental parameters to describe the hydrodynamic behaviour of the modelled BFB.

Table 1 – Mathematical correlations for the modelling of BFB [35].

Name	Expression	
Initial bubble size [cm]	$d_{b0} = \frac{1.30}{g^{0.2}} \left[\frac{u_0 - u_{umf}}{N_{or}} \right]^{0.4}$	(8)
Limiting size of bubble [cm]	$d_{bm} = 0.65 \left[A_{bed} (u_0 - u_{mf}) \right]^{0.4}$	(9)
Bubble diameter [cm] [49]	$d_b = \frac{0.54}{g^{0.2}} (u_0 - u_{mf})^{0.4} \left(z + 4 \left(\frac{A_{bed}}{N_{or}} \right)^{0.5} \right)^{0.8}$	(10)
Minimum fluidising velocity [cm/s]	$u_{mf} = \frac{\mu_g}{\rho_g d_p} (27.2^2 + 0.0408 Ar)^{0.5} - 27.2)$	(11)
Rise velocity of a single bubble [cm/s]	$u_{br} = 0.711 (g\ d_b)^{0.5}$	(12)
Rise velocity for bubbles in bubbling beds [cm/s]	$u_b = u_0 - u_{mf} + u_{br}$	(13)
Rise velocity of emulsion gas	$u_e = \frac{u_{mf}}{\varepsilon_{mf}}$	(14)
The fraction of bed in bubbles, $\frac{m^3\ bubbles}{m^3\ bed}$	δ	
- Vigorously bubbling beds, $u_0 \gg u_{mf}$	$\delta = \frac{u_0}{u_b}$	(15
- Fast bubbles, $u_b > 5 \frac{u_{mf}}{\varepsilon_{mf}}$	$\delta = \frac{u_0 - u_{mf}}{u_b - u_{mf}}$	(16)
- Slow bubbles, $u_b < u_e$	$\delta = \frac{u_0 - u_{mf}}{u_b + 2u_{mf}}$	(17)

- Intermediate bubbles, $\frac{u_{mf}}{\varepsilon_{mf}} < u_b < 5\frac{u_{mf}}{\varepsilon_{mf}}$

$$\delta = \begin{cases} \frac{u_0 - u_{mf}}{u_b + u_{mf}} & when\ u_b \cong \frac{u_{mf}}{\varepsilon_{mf}} \\ \frac{u_0 - u_{mf}}{u_b} & when\ u_b \cong 5\frac{u_{mf}}{\varepsilon_{mf}} \end{cases} \quad (18)$$

Mass interchange coefficient bubble-cloud [s^{-1}]

$$K_{bc} = 4.5\left(\frac{u_{mf}}{d_b}\right) + 5.85\left(\frac{\mathcal{D}_{ij}^{0.5} g^{0.25}}{d_b^{1.25}}\right) \quad (19)$$

Mass interchange coefficient cloud-emulsion [s^{-1}]

$$K_{ce} = 6.77\left(\frac{\mathcal{D}_{ij}\varepsilon_{mf} u_{br}}{d_b^3}\right)^{0.5} \quad (20)$$

Total mass interchange coefficient bubble-emulsion [s^{-1}]

$$\frac{1}{K_{be}} = \frac{1}{K_{bc}} + \frac{1}{K_{ce}} \quad (21)$$

Gas phase diffusivities [cm^2/s] [50]

$$\mathcal{D}_{ij} = \frac{\left(10^{-3} T^{1.75}\left(1/MW_i + 1/MW_j\right)^{0.5}\right)}{p\left[\left(\sum_i v_i\right)^{\frac{1}{3}} + \left(\sum_j v_j\right)^{\frac{1}{3}}\right]^2} \quad (22)$$

Gas viscosity [Pa s] [51]

$$\mu_g = \frac{\sum_i \left(\mu_i x_i MW_i^{0.5}\right)}{\sum_i \left(x_i MW_i^{0.5}\right)} \quad (23)$$

Heat transfer coefficient bubble-cloud [$W/m^3{}_b\,K$]

$$H_{bc} = 4.5\left(\frac{u_{mf}\rho_g c_{pg}}{d_b}\right) + \frac{5.85\left(\lambda_g \rho_g c_{pg}\right)^{0.5} g^{0.25}}{d_b^{1.25}} \quad (24)$$

Heat transfer coefficient cloud-emulsion [$W/m^3{}_b\,K$] [44]

$$H_{ce} = 6.78\left(\frac{\varepsilon_{mf}\lambda_g \rho_g c_{pg} u_b}{MW_g d_b^3}\right)^{0.5} \quad (25)$$

Total heat transfer coefficient bubble-emulsion

$$\frac{1}{H_{be}} = \frac{1}{H_{bc}} + \frac{1}{H_{ce}} \quad (26)$$

2.2.1 Kinetic model

The homogeneous reactions are listed in Table 2 along with their kinetic equations. These take place simultaneously but at different rates, according to the conditions that occur in each compartment. The dependence from the temperature of each kinetic is expressed by the Arrhenius-type equation:

$$k_j = A_j \exp\left(-\frac{Ea_j}{RT}\right) \quad (27)$$

No heterogeneous reactions take place in the freeboard, assuming that fine char particles are rapidly carried over with the gas. The fraction of fine char is produced inside the bed due to comminution of coarse particles [52,53]. Coarse char particles, which have a terminal fall velocity higher than superficial gas velocity, instead, are consumed in the emulsion phase by heterogeneous reactions listed in Table 3.

Table 2 – Homogeneous reactions that occur in the bed gasifier. Reaction rates are expressed in mol/m^{3}s, concentrations in mol/m^3, Activation energy in J/mol.

r_j	Reactions	Reaction rates (mol/m^{3}s)	Ref.
1.	$CO + H_2O \rightleftarrows CO_2 + H_2$	$r_1 = k_1\left(c_{CO}\, c_{H_2O} - \frac{c_{CO_2}\, c_{H_2}}{K_{eq,1}}\right)$ $A_1 = 2.778$ $Ea_1 = 12560$ $K_{eq,1} = 0.022 \exp\left(-\frac{34730}{RT}\right)$	[28]
2.	$CH_4 + H_2O \rightleftarrows CO + 3H_2$	$r_2 = k_2\left(c_{H_2O}\, c_{CH_4} - \frac{c_{CO}\, c_{H_2}^3}{K_{eq,2}}\right)$ $A_2 = 4.916 \cdot 10^{-10} T^2 \cdot \frac{c_C}{M_C \rho_C d_p}$ $Ea_2 = 36150$ $K_{eq,2} = 3.106 \cdot 10^{14} \exp\left(-\frac{208800}{RT}\right)$	[28,54]
3.	$H_2 + \frac{1}{2}O_2 \rightarrow H_2O$	$r_3 = k_3\, c_{O_2}\, c_{H_2}$ $A_3 = 1.08 \cdot 10^{10}$ $Ea_3 = 125525$	[28]
4.	$CO + \frac{1}{2}O_2 \rightarrow CO_2$	$r_4 = k_4\, c_{CO}\, c_{H_2O}^{0.5}\, c_{O_2}^{0.25}$ $A_4 = 1.78 \cdot 10^{10}$ $Ea_4 = 180032$	[28]
5.	$CH_4 + \frac{1}{2}O_2 \rightarrow CO + H_2$	$r_5 = k_5 c_{CH_4}^{0.7} C_{O_2}^{0.8}$ $A_5 = 1.58 \cdot 10^{10}$ $Ea_5 = 202641$	[28]
6.	$CH_4 + 2O_2 \rightarrow CO_2 + H_2O$	$r_6 = k_6\, c_{CH_4}^{0.3}\, c_{O_2}^{1.3}$ $A_6 = 2.06 \cdot 10^{6}$ $Ea_6 = 202500$	[55]
7.	$C_6H_6 + 3O_2 \rightarrow 6CO + 3H_2$	$r_7 = k_7\, c_{C_6H_6}\, c_{O_2}$ $A_7 = 1.58 \cdot 10^{12}$ $Ea_7 = 202641$	[28]
8.	$C_6H_6 + 5H_2O \rightarrow 5CO + 6H_2 + CH_4$	$r_8 = k_8\, c_{C_6H_6}$ $A_7 = 4.4 \cdot 10^{5}$ $Ea_7 = 220000$	[55]
9.	$C_{10}H_8 + 4H_2O \rightarrow C_6H_6 + 4CO + 5H_2$	$r_9 = k_9\, c_{C_{10}H_8}\, c_{H_2}^{0.4}$ $A_9 = 9.97 \cdot 10^{10}$ $Ea_9 = 324000$	[55]
10.	$CH_xO_y + zO_2 \rightarrow \left(\frac{x}{2} - y - 2z + 2\right)CO + \left(y + 2z - \frac{x}{2} - 1\right)CO_2 + \frac{x}{2}H_2O$	$r_{10} = k_{10} c_{O_2} c_{CH_xO_y}$ $A_{10} = 1.58 \cdot 10^{7}$ $Ea_{10} = 201000$	[36]
11.	$Tar \rightarrow products$	$r_{11} = k_{11} c_{Tar}$ $A_{11} = 4 \cdot 10^{4}$ $Ea_{11} = 76600$	[56]

Table 3 – Heterogeneous reactions that occur in the bed gasifier. Reaction rates are expressed in mol/m^{3}s, concentrations in mol/m^3, Activation energy in J/mol.

r_j	Reactions	Reaction rates (mol/m^{3}s) [28,55]	References
12.	$C + CO_2 \rightleftarrows 2CO$	$r_{12} = k_{12}\frac{c_{CO_2}}{1 + K_{k,CO_2}^{(12)} c_{CO_2} + K_{k,CO}^{(12)} c_{CO}}$ $A_{12} = 4.89 \cdot 10^7 \left(\frac{\rho_{char}}{M_{char}}\right)$ $Ea_{12} = 268000$ $K_{k,CO_2}^{(12)} = 6.60 \cdot 10^{-2}$ $K_{k,CO}^{(12)} = 1.2 \cdot 10^{-1} \exp\left(-\frac{25500}{RT}\right)$	[28]
13.	$C + H_2O \rightleftarrows H_2 + CO$	$r_{13} = k_{13}\frac{c_{H_2O}}{1 + K_{k,H_2O}^{(13)} c_{H_2O} + K_{k,H_2}^{(13)} c_{H_2} + K_{k,CO}^{(13)} c_{CO}}$ $A_{13} = 2.39 \cdot 10^2 \left(\frac{\rho_{char}}{M_{char}}\right)$ $Ea_{13} = 129000$ $K_{k,H_2O}^{(13)} = 3.16 \cdot 10^{-2} \exp\left(-\frac{30100}{RT}\right)$ $K_{k,H_2}^{(13)} = 5.36 \cdot 10^{-3} \exp\left(-\frac{59800}{RT}\right)$ $K_{k,CO}^{(13)} = 8.25 \cdot 10^{-5} \exp\left(-\frac{96100}{RT}\right)$	[28]
14.	$\alpha C + O_2 \rightleftarrows 2(\alpha - 1)CO + (2 - \alpha)CO_2$	$r_{14} = k_{14}\, c_{o_2}$ $A_{14} = 5.957 \cdot 10^2 \cdot T_p \left(\frac{6}{d_p}\right)$ $Ea_{14} = 149440$ $\alpha = \frac{1 + 2f_r}{1 + f_r}$ $f_r = 4.72 \cdot 10^{-3} \exp\left(\frac{37737}{RT_p}\right)$	[28]

2.3 Experimental apparatus and procedure

2.3.1 The Pilot Plant

The FBG that was used to generate experimental results for model validation is part of the waste gasification pilot plant based in Swindon (UK). The Swindon plant has been extensively used for R&D purposes and accurate description of plant components and operation is available elsewhere [57,58].

RDF is initially stored in a buffer hopper mounted on load cells and fitted with level indication and alarm. The RDF is extracted from the hopper at a controlled rate using a variable

feed screw. A rotary valve after the variable feed screw provides an airlock before the RDF is fed to the gasifier by a constant speed screw. Gasification takes place in a bubbling fluidised bed gasifier at about 750 °C using steam and oxygen as fluidising gases. During start-up, the system is warmed up to about 600 °C using hot air supplied by a natural gas burner.

The trials began with 75 kg of virgin bed material in the BFB. During the course of the trial, this material was discharged frequently to maintain a bed differential pressure of 50-70 mbar and prevent the build-up of oversize. Bed material, along with any solid residue from gasification of the RDF (e.g., inert glass, metal fractions, etc.) are extracted automatically from the bottom of the bed, cooled, and finally screened using a vibrating screen to separate the sand from the solid residues. Sand is then recycled back to the process. The extracted bed material is metered using a slide gate valve. The slide valve opens for a fixed period of a few seconds, discharging approximately 0.03 m^3 per pulse, the pulsing being used to meter the flow of bed material. The on-line extraction screening and recycle of bed material was not a feature of the model, as their effect on syngas quality is expected to be minimal.

The actual operating conditions of the gasifier depend on fuel characteristics and desired reaction profiles. Bed temperature is controlled to not exceed 850 °C by adjusting steam/oxygen ratio and fuel feed. This is to avoid the risk of incipient ash melting and possible formation of agglomerates, which represent a major issue in RDF gasification. Maintaining a nearly constant bed temperature also helps to minimise reactor upset conditions due to fuel variations (moisture, ash, heating value, etc) providing near steady-state conditions for the performance of the gasifier. The plant is specifically instrumented with direct and continuous measurements of flows, gas composition, temperatures and pressures. The on-line syngas composition was monitored using a Gasmet Fourier Transform Infrared (FTIR) Spectroscopy gas analyser. Additional CO:CO_2 monitoring is undertaken utilising a XEntra 4210 analyser.

The calorific value of the gas and its Wobbe index are monitored using a CWD 2005 Calorimeter.

A schematic diagram of the experimental apparatus is shown in Figure 2. The main design and operation characteristics of the pilot FBG are summarised in Table 4.

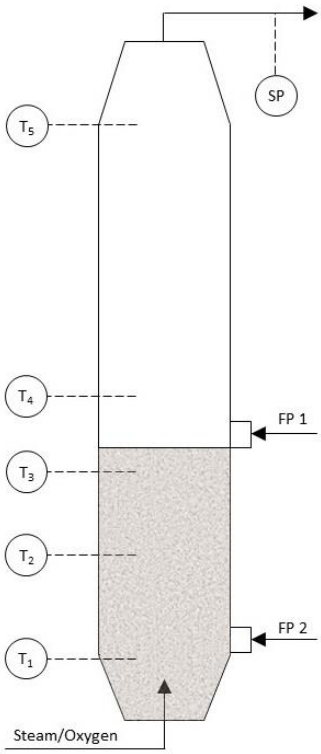

Figure 2 – Schematic diagram of the system with RDF feeding ports (FP): FP1-bottom bed, FP2-top bed, sampling point for gas analysis (SP) and FBG temperatures (T): T_1-bottom bed, T_2-middle bed, T_3-top bed, T_4-splashing zone, T_5-freeboard.

Table 4 – Design and characteristics of the pilot BFB.

Parameter	Values
Bed diameter [m]	0.25
Bed expanded height [m]	1.10
Freeboard height [m]	3.00
Bed temperature [°C]	700-800
Fuel feeding rate [kg/h]	40-60
Oxygen to fuel ratio [wt/wt]	0.28-0.33
Steam to oxygen ratio [mol/mol]	2.5-3
Bed inert material density [kg/dm^3]	2.7
Bed inert material mean diameter [μm]	615

2.3.2 Feedstock characterization

The feedstock used for reference testing was a standard UK municipal solid waste-derived RDF. The prepared RDF comes from several waste treatment facilities in floc form of size ranging from 5 to 50 mm. Table 5 shows the average chemical, mechanical and calorific properties of a RDF sample.

Table 5 – Physical and chemical properties of RDF [59–63].

Property	RDF
Bulk density [kg/m^3]	100-200
Particle size (mm)	5-50
Proximate analysis (wt% fuel as received)	
Fixed Carbon	8.90
Volatile matter	64.70
Ash	11.80
Total moisture	14.60
Ultimate analysis (wt% fuel as received)	
Carbon	41.76
Hydrogen	5.05
Oxygen	23.39
Nitrogen	3.02
Sulphur	0.13
Chlorine	0.25
Energy content (MJ/kg)	
Gross calorific value	21.34
Net calorific value	19.89

The model hypothesis of instantaneous devolatilization of RDF has been investigated through thermo-gravimetric tests. The objective was to determine the reaction kinetic of the RDF primary decomposition to assess the time required for the total conversion (Section 2.1).

A sample of RDF of about 38 mg has been analysed in a lean-oxygen atmosphere (10% O_2 and 90%N_2), similar to typical gasification conditions inside the bed, with a constant heating rate. Several iterations were undertaken at different heating rates, in a range 10-125 °C/min. TGA curve obtained for the RDF is reported in Figure 3. This test was performed using a TGA/DSC 3+ (LF) by Mettler Toledo. The thermogravimetric analyser can perform heating rates in the range 0.02 to 150 °C/min and the balance resolution is 0.1 μg. Products of

devolatilization and gas composition were measured using an online FTIR gas analyser (Rapidox 7100 Multigas Analyser by Sensotec).

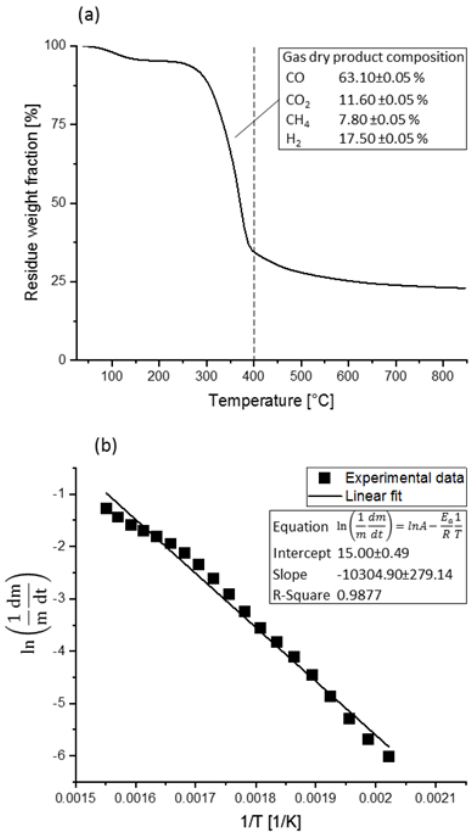

Figure 3 – RDF devolatilization kinetic determination. a) TGA curve in an atmosphere of 10% O_2 and 90% N_2, and gas composition. b) Linearization plot of the Arrhenius-type kinetic equation and experimental data from TGA results.

Through the TGA results, it has been possible to develop a simple gravimetric kinetic equation for thermal degradation reaction of RDF. This is a simplified global model that correlates the rate of RDF consumption to the products (Eq. 1) [64]. It is represented by a single reaction pathway that aims to reproduce the multi-scale physical and chemical transformations that occur during feedstock devolatilization [36]. The final solid residue is composed by the ash and fixed carbon fraction of the RDF and is used for the mass balance expressed by equation 1. Arrhenius first-order rate equation was used to describe the reaction kinetic, where

the calculated activation energy and the pre-exponential factor are $9 \cdot 10^4$ J/mol and $3 \cdot 10^6$ s^{-1} respectively.

3 RESULTS AND DISCUSSION

3.1 Comparison of the model with industrial evidence

The model was first run at inlet condition close to experimental ones, with a margin of error consistent with real plant operation. These correspond to an oxygen to fuel mass ratio and steam to oxygen ratio (SO) of 0.28 and 2.7, respectively. Figure 4 shows the temperature profile of the FBG during operation at the above conditions. While the temperature at different locations in the bed is maintained fairly constant at 750 ºC, a significant increase in temperature was observed, both in the model and experimentally, in the splashing zone right above the bed surface. A similar trend has been observed by Parrillo et al. [65], who measured the axial temperature profile in a pilot scale BFB for biomass gasification. Their results show a maximum temperature in the upper region of the bed and the splashing zone, while after the peak, temperature decrease in the freeboard due to prevalence of endothermic reaction and heat loss [65]. As explained later in Section 3.4, this behaviour is possibly related to the fraction of oxygen that by-passes the bed in the form of fast rising bubbles and reacts in the above zones when bubbles erupt. Temperatures in the freeboard return then to lower values (~780 ºC), in response to endothermic reactions occurring in the gas phase.

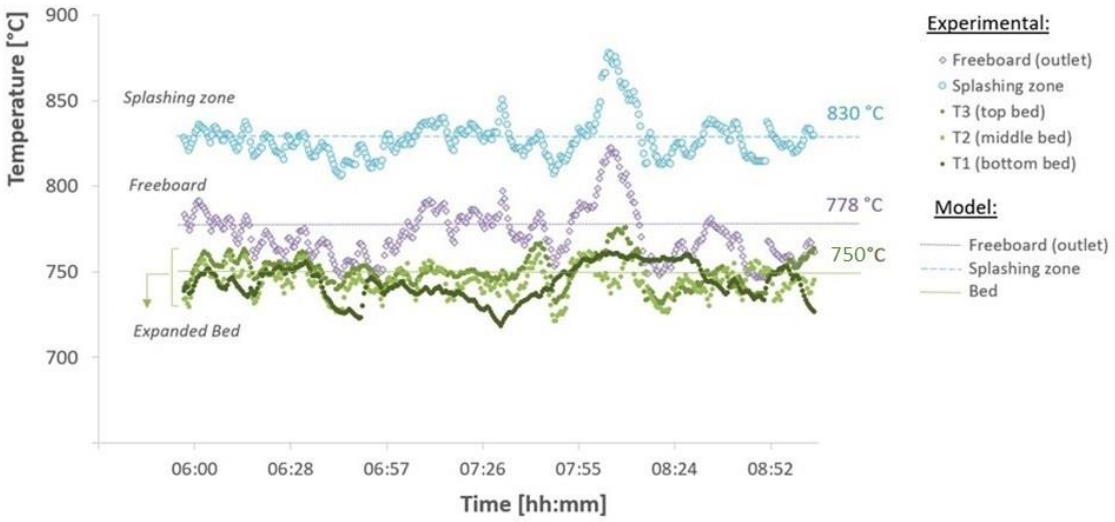

Figure 4 – Experimental and model predicted FBG temperature profile. Thermal input: 300 kW, oxygen/fuel: 0.28, SO: 2.7.

Figure 5 shows the gas composition of the main products and the lower heating value compared to those calculated by the model. Hydrogen molar fraction is around 20%, which compares well to results reported in different studies [66], while carbon monoxide fraction is roughly half. As expected, molar fractions of carbon dioxide and steam are quite high, more than 20% and 30% respectively, which is related to the use of steam-oxygen as gasification agents. The results from the model and the pilot plant compare well with literature data for similar processes [23,66,67]. Differences are justified by the different operating conditions, feedstock and reactor configuration that can be chosen for gasification of waste and residual feedstock, depending on the overall objectives of the plant.

The gas composition is generally well predicted and close to the experimental values, showing a deviation of about 1% between the calculated and experimental data for most species. More relevant discrepancies are related to steam and methane molar fractions (10% and 3% respectively). The difference is mostly due to the high variability of the steam fed into the reactor, and the limited number of species in the model to represent the hydrocarbon distribution. The gross heating value (GHV) is calculated with relation to gases only, while the

measured one might include some residual vapours (steam mostly) in small percentages. This would explain the slightly higher heating value calculated by the model. Normal cubic meters refer to volumes at 0°C and 1atm dry.

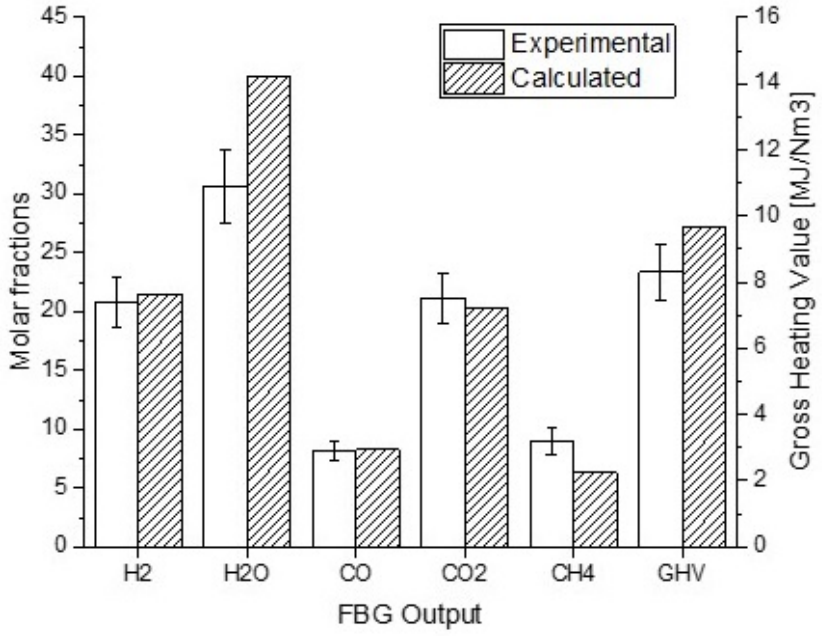

Figure 5 – Comparison of molar gas composition and GHV predicted by the model with experimental data.

The model shows to be reliable also for the evaluation of hydrocarbon species, including methane, benzene and total tars, as shown in Figure 6.

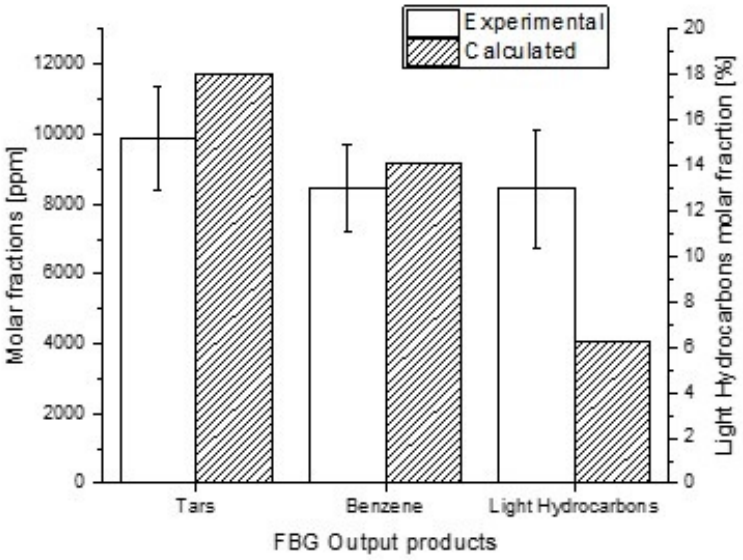

Figure 6 – Comparison of the molar composition of hydrocarbon species predicted by the model with experimental data from FBG.

For completeness and additional information to the reader, the fraction of heavy hydrocarbons (HC) from the plant has been analysed following ASTM D5134 and the product distribution is shown in Figure 7 [68]. Benzene content is also reported as this is present among the permanent gas. Other hydrocarbons have been reported grouping the compounds according to the number of carbons.

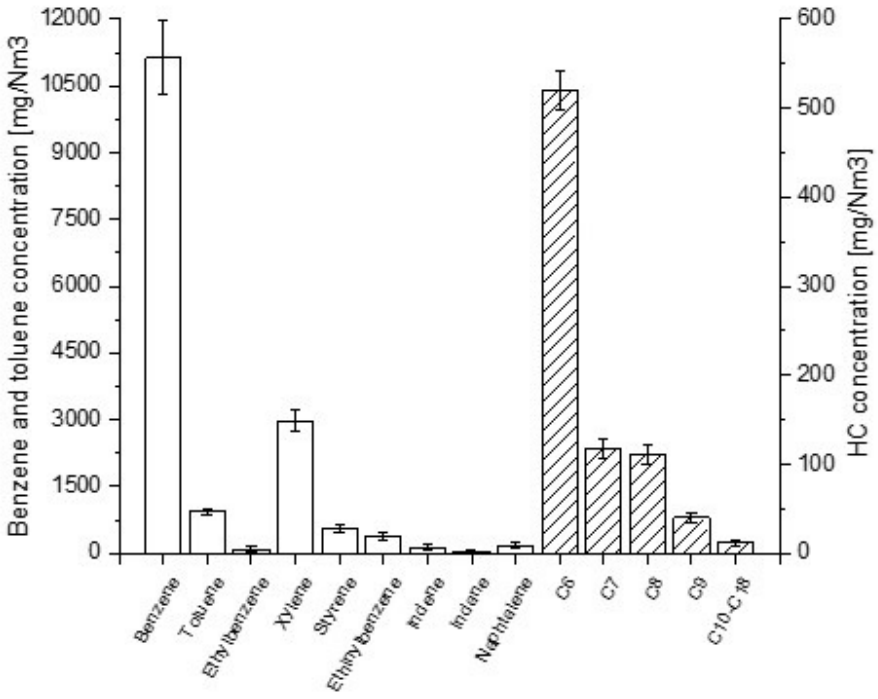

Figure 7 – Analyses of HC's and C6+.

It can be observed that tars content in the syngas obtained from RDF gasification in a stand-alone BFB is significant, requiring additional reforming for syngas utilization.

3.2 Effect of the feeding point

The model was also capable of describing the effect of the feeding height, pointing out the differences between on-bed and in-bed feeding tests (Figure 8). Figure 8a shows the evolution of molar fractions on a dry basis when the feeding height, reported as percentage of the total bed height, varies. By decreasing the height of the feeding point, RDF particles undergo initial devolatilization lower inside the bubbling bed, and therefore the residence time of the species released inside the bed increases. This condition enhances the performance of the reactions and leads to a higher concentration of hydrogen and carbon monoxide in the gas. In particular, the water-gas shift and methane/tars reforming reactions (r_1, r_2, r_8, r_9 in Table 2) play a major role in this [69]. The effect of residence time is well illustrated in Figure 8b, in which both H_2:CO

and $CO:CO_2$ ratios decrease when the RDF is fed at higher levels in the bubbling bed. Figure 8c, instead, shows how the cold gas efficiency (CGE) slightly decreases due to the reduced extent of tar cracking. The lower heating value (LHV) also increases because of the increasing methane concentration that counterbalances the decrease of hydrogen and carbon monoxide, reaching its maximum when RDF is fed from the top of the bed. The choice of the location for the feeding point depends on the specific requirements of the plant. Higher $H_2:CO$ ratios are desirable for fuel synthesis applications, while syngas heating value plays a role of major interest for energy production.

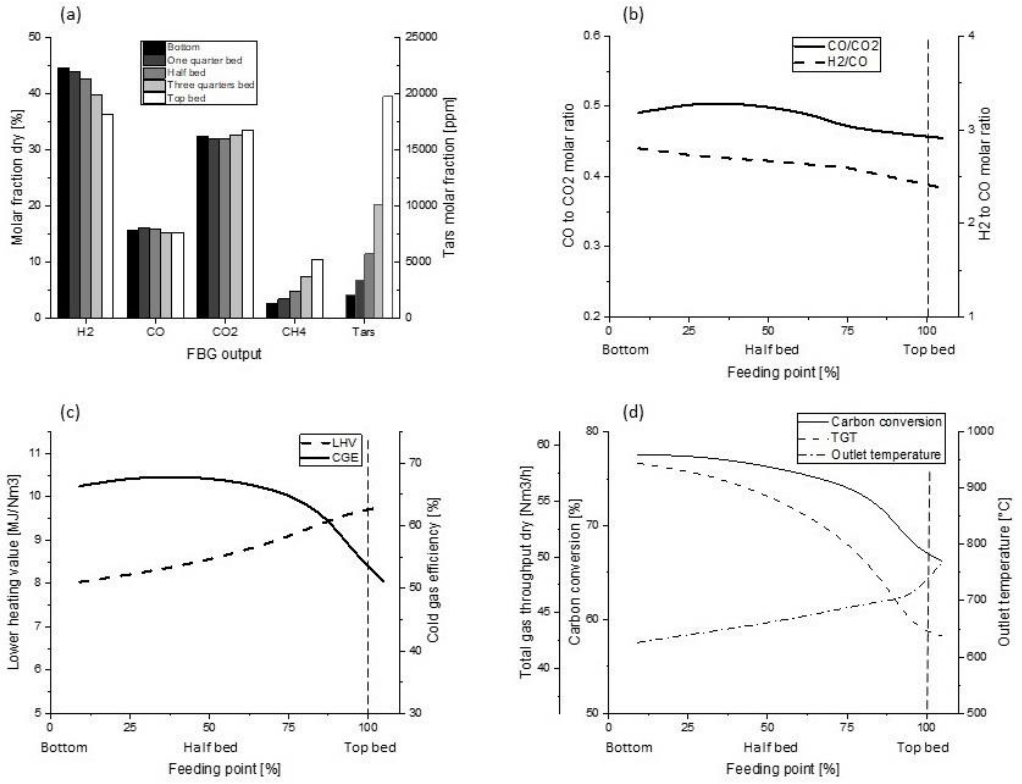

Figure 8 – FBG performance as a function of the feeding height. (a) Main products dry molar fraction at the outlet of the gasifier. (b) $CO:CO_2$ and $H_2:CO$ molar ratios. (c) LHV and CGE. (d) CC and TGT and outlet gas temperature.

Feeding RDF from the top of the bed has seemingly a detrimental effect on tar reforming, which is reflected on lower total gas throughput (TGT) and carbon conversion efficiency (CC)

(Figure 8d). This is expected as a higher tar content means that less carbon ends up into syngas (as CO, CH_4, and CO_2). The outlet stream temperature increases with increasing the feeding height, confirming the effect of lower residence time on both reforming and shift reactions. The outlet temperature is also affected by the extent of combustion reactions that take place in the freeboard rather than inside the bed.

These results suggest some design and operation conclusions with regards to the feeding location of highly volatile materials. While a feeding point at the bottom appears to be the best solution in terms of syngas quality and efficiency (as for CC and TGT), this comes at a high cost, due to increased complexity of feeder design and many operational problems (e.g. backflow of bed and fuel particles, feeder clogging, gas leaks, etc.). On the other hand, an on-bed feeding is much easier to operate and control, and therefore a more favourable option. The limited differences in syngas quality make the easiest-to-operate option also the most suitable.

3.3 Effect of the thermal input

Figure 9 shows the effect of the thermal input, i.e. energy entering the gasifier with the RDF, varying due to changes in feeding rates. When RDF mass rate is increased, the oxygen to fuel ratio and SO are kept constant, which means oxygen and steam feeding rates increase proportionally with the fuel-feeding rate. Increasing the thermal input has two conflicting effects: while more gas is released by devolatilization and made available for reactions, at the same time it decreases the residence time and, therefore, the reaction time. The first effect results in a higher outlet gas flowrate, as shown in Figure 9d. On the other hand, the decreasing residence time entails the reduction of the syngas quality. In particular, Figure 8a shows the variation of the dry molar fractions of hydrocarbon species with the increasing thermal input. Besides the higher amounts of species that are released from the RDF, the reduced residence time results in higher concentrations of hydrocarbon species, due to the limited shift and

reforming reactions (Figure 9a). The experimental data for methane concentration and LHV show the same increasing trend. Figure 9b shows the variation of the syngas quality, in terms of H_2:CO and CO:CO_2 ratios, as a function of the thermal input. These trends are a consequence of the decreasing residence time on shift reactions that cause the concentrations of hydrogen and carbon dioxide to decrease of about 10% each, while that of carbon monoxide increases by roughly 15%. The predicted values compare well with the experimental ones as the calculated values fall within the experimental range of error.

The favourable rise of the gas throughput comes with a higher outlet stream temperature caused mainly by the enhanced combustion reactions (Figure 9d). This implies higher risks for materials resistance, and difficulty to control. The experimental temperatures show the same increasing trend, although with generally lower values. This difference is due to the thermal conductivity of the refractory material, which is assumed to be constant in the model. Interestingly, reducing the thermal input excessively does not result in a specular reduction of tars. Figure 9a shows that average tar content is constant for thermal input below 200 kW in the pilot plant. Furthermore, despite H_2:CO increases rapidly at lower thermal inputs, this is counterbalanced by a reduction of the TGT of the same magnitude, making the CGE unaffected.

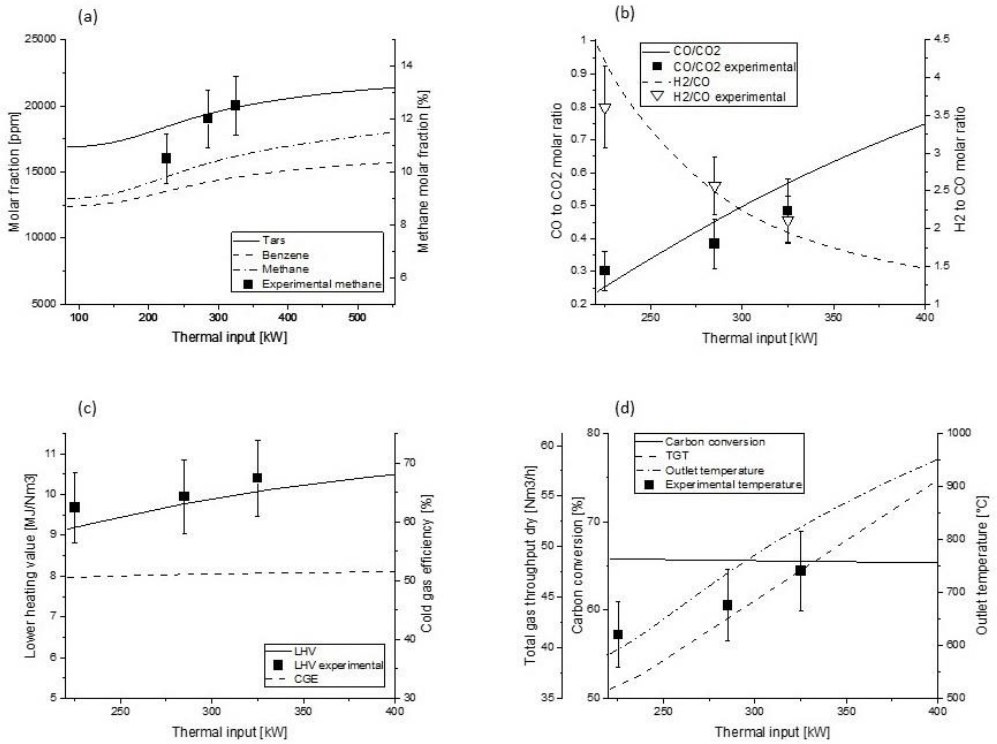

Figure 9 – FBG performance as a function of the thermal input. (a) Dry molar fraction of the hydrocarbon species at the outlet of the gasifier. (b) CO:CO_2 and H_2:CO molar ratios. (c) LHV and CGE. (d) CC and TGT and outlet gas temperature.

Considering the double conflicting effects of rising the thermal input, coupled with the limit imposed by the technology and materials, the model suggests an optimum feeding rate of approximately 40-60 kg/h of RDF for the pilot plant. Notably, the same operational range was confirmed by plant specifications.

3.4 Effect of the equivalent ratio

The equivalent ratio (ER) is defined as the ratio between the oxygen fed to the system and the stoichiometric oxygen required for full combustion. ER is a key parameter for ATT processes like gasification, since this is responsible for the thermal equilibrium of the reactor, in which the temperature has to be sufficiently high for endothermic reactions to occur. Typically, an increase in ER implies that more oxygen is available for combustion reactions,

resulting in an increase in reactor temperature. Since in the model the bed emulsion is assumed to be isothermal, its temperature remains constant and does not vary with changing of operating conditions, including ER. This assumption could possibly limit the predicting capability of the model, and as such it requires further validation. Incidentally, in pilot plant tests, average bed temperature was found to be affected by ER only to a minimum extent. Variations were only evident in the upper region of the bed (T3 in Figure 2), and always lower than ±100°C for the entire range of examined ER (0.2-0.4). This can be explained by the fact that in BFB reactors, a large fraction of the inlet oxygen by-passes the bed and reacts in the freeboard, leaving the bed temperature almost unaffected. This effect is clearly evident when looking at the temperature distribution across the entire reactor (Figure 4), which shows the highest temperature in proximity of the splashing zone, i.e. the region immediately above the bed. For the same reason, freeboard temperature is strongly dependent on ER, playing an important role in determining gasification performance and product gas composition. Figure 9 shows how the performance of the gasifier is affected by a variation of ER, while the bed temperature and SO are maintained constant at 750 ºC and 2.7, respectively. The most evident effect is the hydrocarbon species decrease, as these are further consumed by the combustion reactions occurring in the freeboard (Figure 10a). A secondary effect is the enhancement of the reforming reactions (r_2, r_8, r_9 in Table 2), in response to higher temperature. This let the H_2:CO ratio decrease and CO:CO_2 increase until reaching a maximum value for ER close to 0.3, beyond which any further addition of oxygen makes combustion reactions predominant. This value is in line with what reported by Basu [29,70]. As expected, when higher ERs are adopted complete combustion reactions of both hydrocarbons and hydrogen are favoured, leading to a progressive reduction of CO:CO_2 and H_2:CO ratios as well as an increase of the outlet temperature (Figure 10d). The predicted values compare well with the experimental data both for H_2:CO and CO:CO_2. Similar trends were found for biomass gasification by Parrillo et al.

[65] in a range of ER 0.21-0.35. The experimental outlet temperatures show the same increasing trend. The discrepancies may again be due to an under-estimation of heating losses along the gasifier.

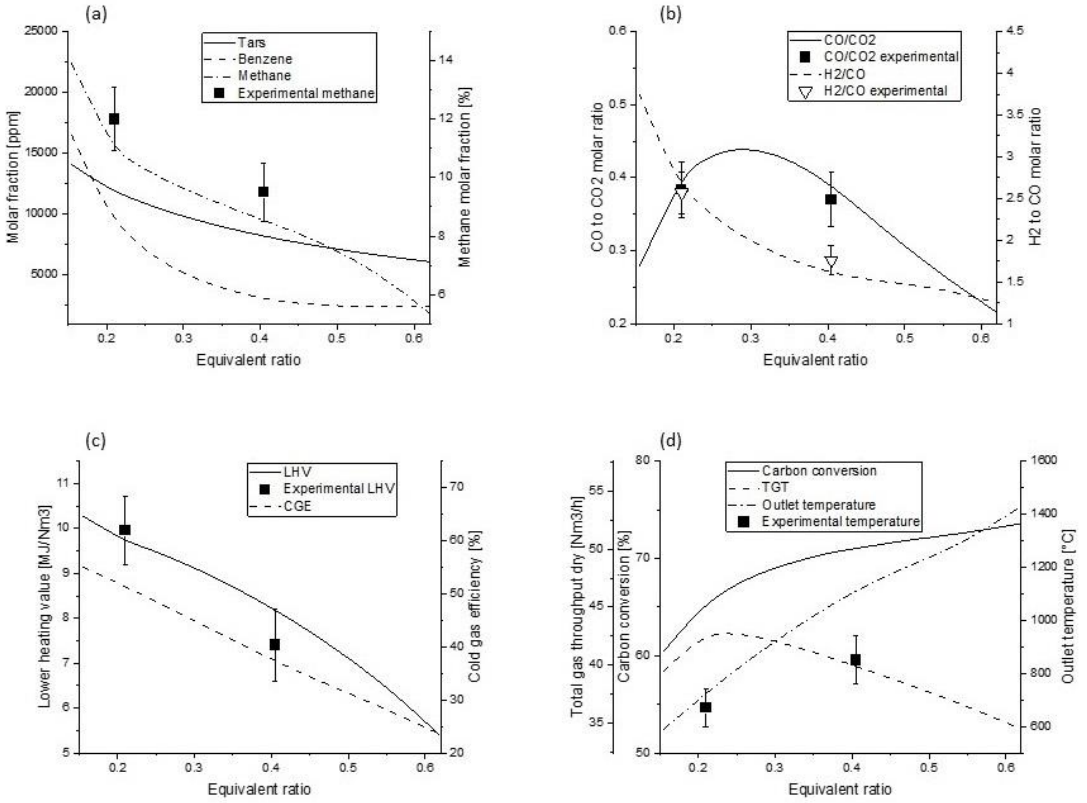

Figure 10 – FBG performance as a function of the ER. (a) Dry molar fraction of the hydrocarbon species at the outlet of the gasifier. (b) CO:CO_2 and H_2:CO molar ratios (c) LHV and CGE. (d) CC and TGT and outlet gas temperature.

The crucial role of the equivalent ratio in thermochemical processes is also shown in Figures 10 c and d. When the oxygen fed is increased, the heating value of the outlet gas stream and the overall CGE decrease significantly, due to the higher fraction of CO_2 and steam produced. In particular, the LHV reaches values over 10 MJ/Nm^3 for low ER (<0.2), while it drops under 6 MJ/Nm^3 for ER higher than 0.6, thus approaching near full combustion conditions. This trend compares well with the experimental values that show an analogous decrease. Within the same range, the CGE decreases of about 30%, approaching zero in case of complete combustion.

Similarly to $CO:CO_2$ ratio, also the TGT in Figure 10d shows a maximum for ER close to 0.25. The increase of combustion reaction with the increasing ER is not reflected by a related growth in the TGT because of the higher quantity of steam that affects the residence time and dilutes the outlet stream. The CC rises when the ER increases as more carbon molecules end up in carbon monoxide and dioxide rather than in tars or heavy hydrocarbons. However, the rate of change is not constant. In particular, for lower values of ER, the CC increases fast with increasing ER, while it is minimally affected for ER higher than 0.3. This effect could be due to soot formation and less reactivity of some tar species at the higher temperatures.

For the purpose of gasification of RDF, the most suitable equivalent ratio suggested by the model appears to be in the range 0.2-0.35.

To further evaluate the predicting capability of the model, a simple sensitivity analysis was run by varying the model FBG bed temperature at the two extreme ER values tested, and at different feeding point locations. A variation of input bed temperature of +/- 50 ºC was shown to have a minimum impact on model predictions, with all main process outputs (LHV, CGE, CC, outlet temperature) varying by less than 5% at ER=0.2, and less than 6% at ER=0.4, with in-bed RDF feeding. No appreciable variations could be observed for the on-bed feeding case.

3.5 Effect of the steam

Steam plays an important role as a fluidising agent in the BFB and for thermal control in RDF gasification. In particular, steam is known to promote reforming and shift reactions while it inhibits combustion reactions. Figure 11 shows the performance of the reactor as a function of the SO. As expected, the most relevant effect is the enhancement of the reforming reactions and the water gas shift (Figure 10a). This results in increasing fractions of hydrogen and carbon dioxide and decreasing carbon monoxide, as confirmed by the experimental measurements. Moreover, steam has a controlling effect on process temperature, inhibiting the combustion

reactions. This is shown in Figure 11b with both heating value and CGE slightly decreasing as steam is increased. The calculated values of the heating values are within the margin of error of the experimental data.

These two conflicting effects of steam, specifically on H_2:CO and LHV, suggest that the optimum ratio can be found in the range 2-3. At the same time, selecting higher values of SO would quench the process, making the control of the autothermal reactor extremely challenging.

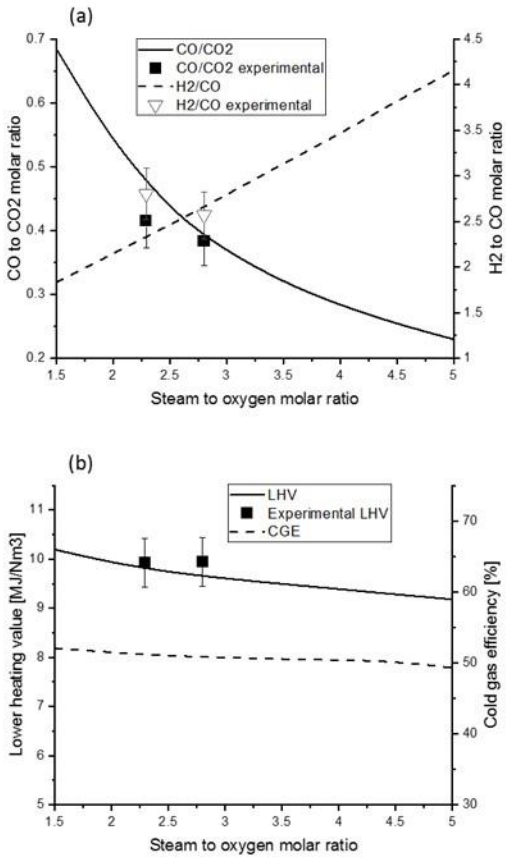

Figure 11 – FBG performance as a function of the SO. (a) CO:CO_2 and H_2:CO molar ratios. (b) LHV and CGE.

4 CONCLUSIONS

A model for the RDF gasification in bubbling fluidised beds has been developed. The model includes kinetics of the main reactions and accounts for the fluid-dynamic of a BFB evaluated

in separated sub-models. The one-dimensional non-isothermal model was used to investigate the performance of a steam-oxygen gasifier and the results were compared with experimental data from tests conducted in a demonstration plant. The model proved to be reliable in the estimation of the output of the gasifier, despite the assumption of mono-dimensional axial variation. This assumption provided ease of computation and less time of simulation compared to available kinetic models. Furthermore, a sensitivity analysis was made to investigate the effects of operating parameters on the system, in order to find the optimum ranges.

The model requires only data for reactor geometry, fuel properties and operational parameters as inputs, while the modular structure allows the model to be modified and easily adapted to each specific case. RDF devolatilization proved to have a crucial role in the process. Unlike the common assumption of instantaneous devolatilization, this step has been investigated separately, and an ad hoc kinetic equation has been developed for standard RDF. Tar released during primary decomposition has been represented by naphthalene and a lumped compound. Secondary tar formation and tar decomposition are also taken into account. The developed model is capable of predicting the product gas composition, tar and char yields and temperature profile in the gasifier under different conditions, showing good agreement with the experimental data. The optimum ranges for thermal input, ER and SO were confirmed by plant specifications. The main limitations of the model involve the lack of radial fuel distribution (including feedstock segregation within the bed) and limited number of kinetic equations. A more realistic fluid dynamic description of the system can only be achieved with more complex models, such as CFD, which however are more difficult to implement. Other limitations are those associated with the two-phase theory (e.g. perfectly mixed and isothermal emulsion phase), which can affect the accuracy of the model when applied to large scale applications. The application to different feedstock (e.g. biomass) is also possible, provided that the fuel specific devolatilization mechanisms are adopted.

This work has also proven that steam-oxygen gasification of RDF could be a valid option to convert waste materials into a more valuable product, representing a possible solution to both the management of unrecyclable waste and alternative fuels production, especially for emerging applications, such as bioSNG and biohydrogen production.

ACKNOWLEDGMENT

The authors wish to acknowledge Dr Richard Taylor and ABSL for having provided the results of the tests and the experimental data necessary for this work.

NOMENCLATURE

Symbols	
A	Pre-exponential factor
A_{bed} [m^3]	Cross-sectional area
Ar	Archimedes number
c [mol/m^3]	Concentration
c_p [J/mol K]	Heat capacity
$\mathcal{D}_{ij}$ [cm^2/s]	Gas phase diffusivities
Ea [J/mol]	Activation energy
g [m/s^2]	Gravity acceleration
H [$W/m^3{}_b$ K]	Heat transfer coefficient
ΔH^r [J/mol]	Reaction enthalpy change
k	Kinetic coefficient
K [s^{-1}]	Mass interchange coefficient
K_{eq}	Equilibrium constant
K_k[1/atm]	Adsorption constant
M [kg]	Mass
MW [g/mol]	Molecular weight
N_{or}	Number of orifices
p [bar]	Pressure
R [J/mol K]	Universal gas constant
R_{tot} [Km^3/W]	Total thermal resistance
r [mol/m^3s]	Reaction rate
T [K]	temperature
u [cm/s]	Velocity
u_0 [cm/s]	Superficial gas velocity
u_{br} [cm/s]	Rise velocity of a single bubble
v	Diffusion volume
x	Molar fraction

z [cm]	Axial position

Greek letters	
δ [m^3_b/m^3_{bed}]	Fraction of bed in bubbles
ε	Void fraction
ν	Stoichiometric ratio
μ [Pa s]	Gas viscosity
ρ [kg/m^3]	Density
λ [W/m K]	Thermal conductivity

Subscripts	
0	Initial
a	Ambient
b	Bubble phase
C	Carbon (in kinetic rate expression)
c	Cloud phase
e	Emulsion phase
eq	Equilibrium
f	Freeboard
g	Gas phase
i	Number of species
j	Reaction number
m	Maximum
mf	Minimum fluidization
p	Particle

Acronyms	
ATT	Advanced thermochemical technologies
BFB	Bubbling fluidised bed
bioSNG	Bio-substitute natural gas
CC	Carbon conversion
CGE	Cold gas efficiency
ER	Equivalent ratio
FBG	Fluidized bed gasifier
FP	Feeding port
FTIR	Fourier transform infrared
GHV	Gross heating value
HC	Heavy hydrocarbons
LHV	Lower heating value
MSW	Municipal solid waste
RDF	Refuse derived fuel
SO	Steam to oxygen ratio
SP	Sampling point
TGA	Thermogravimetric analysis

TGT	Total gas throughput

REFERENCES

[1] N. Ferronato, V. Torretta, Waste mismanagement in developing countries: A review of global issues, Int. J. Environ. Res. Public Health. 16 (2019). https://doi.org/10.3390/ijerph16061060.

[2] A. Welfle, P. Thornley, M. Röder, A review of the role of bioenergy modelling in renewable energy research & policy development, Biomass and Bioenergy. 136 (2020). https://doi.org/10.1016/j.biombioe.2020.105542.

[3] P. Lettieri, L. Yassin, S.J.R. Simons, Advanced thermal treatment of composite wastes for energy recovery, in: Manag. Recycl. Reuse Waste Compos., 2009. https://doi.org/10.1533/9781845697662.2.152.

[4] L. Lombardi, E. Carnevale, A. Corti, A review of technologies and performances of thermal treatment systems for energy recovery from waste, Waste Manag. (2015). https://doi.org/10.1016/j.wasman.2014.11.010.

[5] C.E. Agu, B.M.E. Moldestad, C. Pfeifer, Assessment of Combustion and Gasification Behavior in a Bubbling Fluidized Bed Reactor: A Comparison between Biomass with and without Chemical Additives, Energy and Fuels. 34 (2020) 9654–9663. https://doi.org/10.1021/acs.energyfuels.0c01408.

[6] a. Bosmans, I. Vanderreydt, D. Geysen, L. Helsen, The crucial role of Waste-to-Energy technologies in enhanced landfill mining: A technology review, J. Clean. Prod. 55 (2013) 10–23. https://doi.org/10.1016/j.jclepro.2012.05.032.

[7] A.C. Caputo, P.M. Pelagagge, RDF production plants: I Design and costs, Appl. Therm.

Eng. 22 (2002) 423–437. https://doi.org/10.1016/S1359-4311(01)00100-4.

[8] U. Arena, Process and technological aspects of municipal solid waste gasification. A review, Waste Manag. 32 (2012) 625–639. https://doi.org/10.1016/j.wasman.2011.09.025.

[9] E. Savuto, A. Di Carlo, K. Gallucci, A. Di Giuliano, S. Rapagnà, Steam gasification of lignite and solid recovered fuel (SRF) in a bench scale fluidized bed gasifier, Waste Manag. 114 (2020) 341–350. https://doi.org/10.1016/j.wasman.2020.07.016.

[10] D. Krause, P. Herdel, J. Ströhle, B. Epple, HTW^{TM}-gasification of high volatile bituminous coal in a 500 kWth pilot plant, Fuel. 250 (2019) 306–314. https://doi.org/10.1016/j.fuel.2019.04.014.

[11] C. Courson, K. Gallucci, Gas cleaning for waste applications (syngas cleaning for catalytic synthetic natural gas synthesis), in: Substit. Nat. Gas from Waste, Elsevier, 2019: pp. 161–220. https://doi.org/10.1016/B978-0-12-815554-7.00008-8.

[12] H. Thunman, M. Seemann, T. Berdugo Vilches, J. Maric, D. Pallares, H. Ström, G. Berndes, P. Knutsson, A. Larsson, C. Breitholtz, O. Santos, Advanced biofuel production via gasification – lessons learned from 200 man-years of research activity with Chalmers' research gasifier and the GoBiGas demonstration plant, Energy Sci. Eng. (2018). https://doi.org/10.1002/ese3.188.

[13] M. Materazzi, R. Taylor, M. Cairns-Terry, Production of biohydrogen from gasification of waste fuels: Pilot plant results and deployment prospects, Waste Manag. (2019). https://doi.org/10.1016/j.wasman.2019.05.038.

[14] M. Materazzi, R. Taylor, P. Cozens, C. Manson-Whitton, Production of BioSNG from waste derived syngas: Pilot plant operation and preliminary assessment, Waste Manag.

79 (2018) 752–762. https://doi.org/https://doi.org/10.1016/j.wasman.2018.08.031.

[15] B. Rehling, H. Hofbauer, R. Rauch, C. Aichernig, BioSNG-process simulation and comparison with first results from a 1-MW demonstration plant, Biomass Convers. Biorefinery. 1 (2011) 111–119. https://doi.org/10.1007/s13399-011-0013-3.

[16] M. Materazzi, P.U. Foscolo, The role of waste and renewable gas to decarbonize the energy sector, in: Substit. Nat. Gas from Waste Tech. Assess. Ind. Appl. Biochem. Thermochem. Process., 2019. https://doi.org/10.1016/B978-0-12-815554-7.00001-5.

[17] M. Materazzi, R. Taylor, The GoGreenGas case in the UK, in: M. Materazzi, P.U. Foscolo (Eds.), Substit. Nat. Gas from Waste, Academic Press (Elsevier), 2019: pp. 475–495.

[18] U. Arena, F. Di Gregorio, Fluidized bed gasification of industrial solid recovered fuels, Waste Manag. 50 (2016) 86–92. https://doi.org/https://doi.org/10.1016/j.wasman.2016.02.011.

[19] O. Senneca, R. Chirone, L. Cortese, P. Salatino, Pyrolysis and combustion of a solid refinery waste, Fuel. 267 (2020). https://doi.org/10.1016/j.fuel.2020.117258.

[20] H. Hofbauer, M. Materazzi, Waste gasification processes for SNG production, in: Substit. Nat. Gas from Waste, Elsevier, 2019: pp. 105–160. https://doi.org/10.1016/B978-0-12-815554-7.00007-6.

[21] J.C. Schmid, F. Benedikt, J. Fuchs, A.M. Mauerhofer, S. Müller, H. Hofbauer, Syngas for biorefineries from thermochemical gasification of lignocellulosic fuels and residues—5 years' experience with an advanced dual fluidized bed gasifier design, Biomass Conversion and Biorefinery, 2019. https://doi.org/10.1007/s13399-019-00486-2.

[22] M. Haaf, J. Hilz, J. Peters, A. Unger, J. Ströhle, B. Epple, Operation of a 1 MWth calcium looping pilot plant firing waste-derived fuels in the calciner, Powder Technol. 372 (2020) 267–274. https://doi.org/10.1016/j.powtec.2020.05.074.

[23] M. Campoy, A. Gómez-Barea, P. Ollero, S. Nilsson, Gasification of wastes in a pilot fluidized bed gasifier, Fuel Process. Technol. 121 (2014) 63–69. https://doi.org/10.1016/j.fuproc.2013.12.019.

[24] M.R. Mahishi, D.Y. Goswami, Thermodynamic optimization of biomass gasifier for hydrogen production, Int. J. Hydrogen Energy. 32 (2007) 3831–3840. https://doi.org/10.1016/j.ijhydene.2007.05.018.

[25] M. Moneti, A. Di Carlo, E. Bocci, P.U. Foscolo, M. Villarini, M. Carlini, Influence of the main gasifier parameters on a real system for hydrogen production from biomass, Int. J. Hydrogen Energy. (2016). https://doi.org/10.1016/j.ijhydene.2016.05.171.

[26] M. Materazzi, P. Lettieri, L. Mazzei, R. Taylor, C. Chapman, Thermodynamic modelling and evaluation of a two-stage thermal process for waste gasification, Fuel. 108 (2013) 356–369.

[27] A. Aghaalikhani, J.C. Schmid, D. Borello, J. Fuchs, F. Benedikt, H. Hofbauer, F. Rispoli, U.B. Henriksen, Z. Sárossy, L. Cedola, Detailed modelling of biomass steam gasification in a dual fluidized bed gasifier with temperature variation, Renew. Energy. 143 (2019) 703–718. https://doi.org/10.1016/j.renene.2019.05.022.

[28] I. Petersen, J. Werther, Experimental investigation and modeling of gasification of sewage sludge in the circulating fluidized bed, Chem. Eng. Process. Process Intensif. 44 (2005) 717–736. https://doi.org/10.1016/j.cep.2004.09.001.

[29] P. Basu, Biomass Gasification Design Handbook, 2010. https://doi.org/10.1016/B978-

0-12-374988-8.00005-2.

[30] B. Hejazi, J.R. Grace, X. Bi, A. Mahecha-Botero, Kinetic Model of Steam Gasification of Biomass in a Dual Fluidized Bed Reactor: Comparison with Pilot-Plant Experimental Results, Energy and Fuels. 31 (2017) 12141–12155. https://doi.org/10.1021/acs.energyfuels.7b01833.

[31] O. Oyedeji, N. Abdoulmoumine, Computational fluid dynamics and discrete element simulation of the formation of inorganic syngas contaminants during lignocellulosic biomass gasification, Sustain. Energy Fuels. (2020). https://doi.org/10.1039/d0se00705f.

[32] C.E. Agu, C. Pfeifer, M. Eikeland, L.A. Tokheim, B.M.E. Moldestad, Detailed One-Dimensional Model for Steam-Biomass Gasification in a Bubbling Fluidized Bed, Energy and Fuels. (2019). https://doi.org/10.1021/acs.energyfuels.9b01340.

[33] P. Kaushal, J. Abedi, N. Mahinpey, A comprehensive mathematical model for biomass gasification in a bubbling fluidized bed reactor, Fuel. 89 (2010) 3650–3661. https://doi.org/10.1016/j.fuel.2010.07.036.

[34] A. Gómez-Barea, B. Leckner, Estimation of gas composition and char conversion in a fluidized bed biomass gasifier, Fuel. 107 (2013) 419–431. https://doi.org/10.1016/j.fuel.2012.09.084.

[35] D. Kunii, O. Levenspiel, Fluidization Engineering, 1991. https://doi.org/10.1016/b978-0-7506-9121-5.50001-x.

[36] A. Gomez-Barea, B. Leckner, Modeling of biomass gasification in fluidized bed, 36 (2010) 444–509. https://doi.org/10.1016/j.pecs.2009.12.002.

[37] P. Basu, P. Kaushal, Modeling of Pyrolysis and Gasification of Biomass in Fluidized

Beds: A Review, Chem. Prod. Process Model. 4 (2009). https://doi.org/10.2202/1934-2659.1338.

[38] R. Di Felice, G. Coppola, S. Rapagna, N. Jand, Modeling of biomass devolatilization in a fluidized bed reactor, Can. J. Chem. Eng. 77 (1999) 325–332. https://doi.org/10.1002/cjce.5450770219.

[39] H.J. Huang, S. Ramaswamy, Modeling biomass gasification using thermodynamic equilibrium approach, Appl. Biochem. Biotechnol. 154 (2009) 193–204. https://doi.org/10.1007/s12010-008-8483-x.

[40] G. Gautam, S. Adhikari, S. Bhavnani, Estimation of biomass synthesis gas composition using equilibrium modeling, Energy and Fuels. 24 (2010) 2692–2698. https://doi.org/10.1021/ef901477c.

[41] E.G. Hertwich, X. Zhang, Concentrating-solar biomass gasification process for a 3rd generation biofuel, Environ. Sci. Technol. 43 (2009) 4207–4212. https://doi.org/10.1021/es802853g.

[42] V. Cozzani, C. Nicolella, L. Petarca, M. Rovatti, L. Tognotti, A Fundamental Study on Conventional Pyrolysis of a Refuse-Derived Fuel, Ind. Eng. Chem. Res. 34 (1995) 2006–2020. https://doi.org/10.1021/ie00045a010.

[43] V. Claude, J.G. Mahy, S. Douven, S.L. Pirard, C. Courson, S.D. Lambert, Ni- and Fe-doped γ-Al2O3 or olivine as primary catalyst for toluene reforming, Mater. Today Chem. 14 (2019) 100197. https://doi.org/10.1016/j.mtchem.2019.100197.

[44] W.-C. Yang, Handbook of fluidization and fluid-particle systems, 2008. https://doi.org/10.1016/s1672-2515(07)60126-2.

[45] R. Chirone, L. Massimilla, P. Salatino, Comminution of carbons in fluidized bed

combustion, Prog. Energy Combust. Sci. 17 (1991) 297–326. https://doi.org/10.1016/0360-1285(91)90006-9.

[46] U. Arena, R. Chirone, M. D'Amore, M. Miccio, P. Salatino, Some issues in modelling bubbling and circulating fluidized-bed coal combustors, Powder Technol. 82 (1995) 301–316. https://doi.org/10.1016/0032-5910(94)02933-F.

[47] S. Iannello, S. Morrin, M. Materazzi, Fluidised Bed Reactors for the Thermochemical Conversion of Biomass and Waste, KONA Powder Part. J. (2020). https://doi.org/10.14356/kona.2020016.

[48] R.H. Perry, D.W. Green, J.O. Maloney, Perry's Chemical Engineer's Handbook, 8th ed., McGraw-Hill Education, 2007. https://doi.org/10.1036/0071422943.

[49] R.C. Darton, R.D. LaNauze, J.F. Davidson, D. Harrison, Bubble Growth Due To Coalescence in Fluidised Beds., Trans Inst Chem Eng. 55 (1977) 274–280.

[50] E.N. Fuller, P.D. Schettler, J.C. Giddings, A NEW METHOD FOR PREDICTION OF BINARY GAS-PHASE DIFFUSION, (n.d.). https://doi.org/10.1021/ie50677a007.

[51] T.A. Davidson, Report of Investigations 9456 - A simple and accurate method for calculatlng viscosity of gaseous mixtures, Rep. Investig. UNITED STATES Dep. Inter. (1993) 1–12.

[52] F. Scala, R. Chirone, P. Salatino, 6 - Attrition phenomena relevant to fluidized bed combustion and gasification systems, in: F. Scala (Ed.), Fluid. Bed Technol. Near-Zero Emiss. Combust. Gasif., Woodhead Publishing, 2013: pp. 254–315. https://doi.org/https://doi.org/10.1533/9780857098801.1.254.

[53] U. Arena, R. Chirone, P. Salatino, The fate of fixed carbon during the fluidized-bed combustion of a coal and two waste-derived fuels, Symp. Combust. 26 (1996) 3243–

3251. https://doi.org/10.1016/S0082-0784(96)80170-6.

[54] Y. Wang, C.M. Kinoshita, KINETIC MODEL OF BIOMASS GASIFICATION, 51 (1993) 19–25.

[55] F. Marias, R. Demarthon, A. Bloas, J.P. Robert-Arnouil, F. Nebbad, Design of a High Temperature Reactor Fed by a Plasma Torch for Tar Conversion: Comparison Between CFD Modelling and Experimental Results, Waste and Biomass Valorization. 6 (2014) 97–108. https://doi.org/10.1007/s12649-014-9331-6.

[56] P. Morf, P. Hasler, T. Nussbaumer, Mechanisms and kinetics of homogeneous secondary reactions of tar from continuous pyrolysis of wood chips, Fuel. 81 (2002) 843–853. https://doi.org/10.1016/S0016-2361(01)00216-2.

[57] M. Materazzi, P. Lettieri, L. Mazzei, R. Taylor, C. Chapman, Fate and behavior of inorganic constituents of RDF in a two stage fluid bed-plasma gasification plant, Fuel. 150 (2015). https://doi.org/10.1016/j.fuel.2015.02.059.

[58] M. Materazzi, R. Taylor, P. Cozens, C. Manson-Whitton, Production of BioSNG from waste derived syngas: Pilot plant operation and preliminary assessment, Waste Manag. (2018). https://doi.org/10.1016/j.wasman.2018.08.031.

[59] BSI, Solid recovered fuels — Determination of moisture content using the oven dry method. Part 3: Moisture in general analysis sample., (2009).

[60] BS, BSI Standards Publication Solid biofuels — Determination of the content of volatile matter, (2017).

[61] BSI, BSI Standards Publication Solid recovered fuels — Determination of bulk density, (2010).

[62] BSI, BSI Standards Publication Solid recovered fuels — Methods for the determination

of carbon (C), hydrogen (H) and nitrogen (N) content, (2011).

[63] BSI, BSI Standards Publication Solid biofuels — Determination of ash content, (2017).

[64] G. Skodras, P. Grammelis, P. Basinas, M. Prokopidou, E. Kakaras, G.P. Sakellaropoulos, A thermochemical conversion study on the combustion of residue-derived fuels, Water, Air, Soil Pollut. Focus. 9 (2009) 151–157. https://doi.org/10.1007/s11267-008-9197-3.

[65] F. Parrillo, F. Ardolino, G. Calì, D. Marotto, A. Pettinau, U. Arena, Fluidized bed gasification of eucalyptus chips: Axial profiles of syngas composition in a pilot scale reactor, Energy. 219 (2021) 119604. https://doi.org/10.1016/j.energy.2020.119604.

[66] U. Arena, L. Zaccariello, M.L. Mastellone, Fluidized bed gasification of waste-derived fuels, Waste Manag. 30 (2010) 1212–1219. https://doi.org/10.1016/j.wasman.2010.01.038.

[67] F. Benedikt, J.C. Schmid, J. Fuchs, A.M. Mauerhofer, S. Müller, H. Hofbauer, Fuel flexible gasification with an advanced 100 kW dual fluidized bed steam gasification pilot plant, Energy. 164 (2018) 329–343. https://doi.org/10.1016/j.energy.2018.08.146.

[68] ASTM, Standard Test Method for Detailed Analysis of Petroleum Naphthas through n-Nonane by Capillary Gas Chromatography, 98 (2014) 1–12. https://doi.org/10.1520/D5134-13.

[69] V. Wilk, J.C. Schmid, H. Hofbauer, Influence of fuel feeding positions on gasification in dual fluidized bed gasifiers, Biomass and Bioenergy. 54 (2013) 46–58. https://doi.org/10.1016/j.biombioe.2013.03.018.

[70] P. Basu, Biomass Gasification, Pyrolysis and Torrefaction: Practical Design and Theory, 2013. https://doi.org/10.1016/C2011-0-07564-6.